Signal-to-noise errors in early winter Euro-Atlantic predictions caused by weak ENSO teleconnections and pervasive North Atlantic jet biases

Christopher H. O'Reilly

Department of Meteorology, University of Reading, United Kingdom.

Corresponding author: Christopher H. O'Reilly, c.h.oreilly@reading.ac.uk

Abstract

Long-range winter predictions over the Euro-Atlantic sector have demonstrated significant skill but suffer from systematic signal-to-noise errors. In this study we examine early winter seasonal predictability in 16 state-of-the-art seasonal forecasting systems. Models demonstrate skill in the hindcasts of the large-scale atmospheric circulation in early winter, which mostly projects onto the East Atlantic pattern. The predictability is strongly tied to the ENSO teleconnection to the North Atlantic, though the models' response to ENSO is systematically too weak. The model hindcasts of the East Atlantic index exhibit a substantial signal-to-noise errors, with the models predicted signal generally being smaller than would be expected for the observed level of skill. The signal-to-noise errors are found to be strongly dependent on the strength of the ENSO teleconnection in the models, with models with a weaker teleconnection displaying a larger signal-to-noise problem. It is demonstrated that the dependency on model ENSO teleconnection strength can be explained using a simple scaling relationship derived from a toy model. Further analysis reveals that the strength of the ENSO teleconnection in the model is linked to climatological biases in the behaviour of the North Atlantic jet. Models that better represent the dynamics of the jet over the northern part of the basin - with more frequent poleward jet excursions and less frequent Greenland blocking - are better at representing the ENSO teleconnection to the North Atlantic in early winter, with lower associated signal-to-noise errors.

1. Introduction

The variability in wintertime climate over Europe, as well as parts of North America, is strongly controlled by variability in the large-scale atmospheric circulation over the extratropical North Atlantic. As a result, there is substantial interest in long-range, or "seasonal", forecasts (i.e. lead times of a month or more) of these large-scale circulation anomalies. Historically, long-range forecast skill over the North Atlantic had proven to be elusive (e.g. Johansson 2007; Smith et al. 2012). However, more recent forecast models have demonstrated increased levels of skill over the North Atlantic (e.g. Scaife et al. 2014; Dunstone et al. 2016; Baker et al. 2018), opening up new avenues for the application of these long-range forecasts (e.g. Clark et al. 2017; Thornton et al. 2019; Stringer et al. 2020). Previous studies have largely focussed on understanding the long-range prediction skill of the North Atlantic Oscillation because it is the dominant mode of large-scale circulation variability over the Euro-Atlantic sector (e.g. Hurrell et al. 2003). However, is has recently been shown that early winter (i.e. November-December, ND) predictions of the East Atlantic pattern (EA), the second largest mode of large-scale circulation variability over the Euro-Atlantic sector, are skillful in many state-of-the-art seasonal forecasting systems (Thornton et al. 2023).

The main source of skill in long-range predictions of early winter Euro-Atlantic circulation variability is the El Niño-Southern Oscillation phenomena (ENSO) in the Tropical Pacific ocean (Thornton et al. 2023). During early winter, ENSO variability is strongly correlated with variability in the EA pattern over the North Atlantic (Ayarzagüena et al. 2018; King et al. 2018), with El Niño years projecting onto a positive phase of the EA, bringing significantly milder and wetter conditions to western Europe, with the opposite conditions typically occurring in La Niña years. The influence of ENSO on the EA pattern in early winter is characterised by the suppression of poleward jet excursions during El Niño years and a zonal extension of the jet (O'Reilly et al., *submitted to QJRMS*). Recent studies show that whilst the ENSO teleconnection to the North Atlantic in early winter, specifically the link between ENSO and the EA pattern, is robustly reproduced by state-of-the-art seasonal forecasting systems, the teleconnection in the models is much weaker than that observed in reanalysis datasets (Molteni and Brookshaw 2023; Thornton et al. 2023). However, the underlying causes for the weak teleconnection, and the associated weak forecast signals, remain unclear.

Weak signals in long-range forecasts of the extratropical large-scale circulation are not unique to the early winter North Atlantic. Previous studies have shown that broadly similar problems exist for later winter seasonal forecasts (e.g. Scaife et al. 2014; Dunstone et al. 2016; Baker et al. 2018), subseasonal forecasts over the North Pacific (Garfinkel et al. 2022), decadal forecasts of the wintertime North Atlantic (e.g. Smith et al. 2019, 2020; Marcheggiani et al. 2023), summertime seasonal forecasts over the North Atlantic (e.g. Dunstone et al. 2018, 2023), and may also be related to deficiencies in decadal large-scale circulation variability in free-running climate model simulations (e.g. Bracegirdle et al. 2018; Simpson et al. 2018; O'Reilly et al. 2019, 2021). These signal-to-noise errors have collectively been dubbed the "signal-to-noise problem" (or "signal-to-noise paradox") in the climate science literature (Scaife and Smith 2018). The signal-to-noise problem is a major challenge within climate science as these errors significantly limit confidence in regional climate predictions made using model simulations, over a range of timescales.

A number of theories for the underlying cause, or causes, of the signal-to-noise problem have been proposed. Recent studies have pointed to insufficient atmospheric eddy feedback in models, possibly due to low atmospheric resolution, being a potential deficiency responsible the weak predicted signal in models (Scaife et al. 2019; Hardiman et al. 2022). Some studies have suggested that the misrepresentation of regime persistence as a possible explanation of the signal-to-noise problem (Strommen and Palmer 2019; Strommen 2020). Other studies have indicated that models are lacking in their response to specific predictable drivers, such as those associated with mid-latitude ocean-atmosphere interactions (Ossó et al. 2020; Zhang et al. 2021) or low-frequency variability in the stratosphere (O'Reilly et al. 2019; Charlton-Perez et al. 2019). These are not all mutually exclusive and may be of varying importance in the different manifestations of the signal-to-noise problem. Despite there being a number of proposed theories, there remains considerable uncertainty about the origins of the the signal-to-noise problem in extratropical circulation variability.

In this study we analyse the predictability of the large-scale circulation over the North Atlantic in a suite of seasonal forecasting systems, aiming to understand the causes of the signal-to-noise errors in the early winter predictions. We find that for all the systems, the majority of the seasonal forecast skill during this period can be attributed to the ENSO teleconnection but the ENSO teleconnection is too weak in the models. The strength of the teleconnection is shown to account for the variation of the signal-to-noise ratios across the systems, and this scaling can be explained using a toy model of the forecasts. The strength of the ENSO teleconnection is shown to be linked to pervasive biases in the North Atlantic jet - models whose climatological behaviour is are closer to observations are found to have a stronger ENSO teleconnection to the North Atlantic and reduced signal-to-noise issues. These findings provide useful benchmarks for the improvement of operational seasonal forecasting systems and the identification of signal-to-noise errors in other instances.

2. Datasets & Methods

a. Reanalysis data

We use the ERA5 reanalysis dataset as the reference dataset in the analysis that follows. ERA5 is a state-of-the-art reanalysis produced by ECMWF (Hersbach et al. 2020). ERA5 data is used over the period 1950-2020, comprising 71 winters in total and a shorter period that is the same as the C3S hindcasts, 1993-2016 is also used in places.

b. Seasonal forecast models

In this study we analyse hindcasts data from a total of 16 seasonal forecasting systems, from 8 different interational forecasting centres, that are stored in the C3S multi-model archive (see Table 1 for details). These include many of the current operational system and some previously operational systems. We have chosen to analyse all the models in the C3S archive that have hindcasts covering the common period 1993-2016 (i.e. 24 winters) with initilialisation dates on or before 1st October. Our analysis focuses on the early winter period, November and December, that has been shown to have substantial skill in the hindcasts (Thornton et al. 2023), which is at least in part is due to the strong ENSO teleconnection to the North Atlantic during the early winter (e.g. Ayarzagüena et al. 2018). The models vary in ensemble size from 10 to 42 members. The C3S hindcast datasets were regridded to a common 2.5°×2.5° grid for the analysis with the exception of the eddy-driven jet latitiude diagnostics, which were performed using U_{850} data regridded to a 1°×1° grid.

c. ENSO index

We use the "Oceanic Nino Index" methodology of NOAA to define ENSO years, the HadISST dataset (Rayner et al. 2003). The ONI methodology used three-month averages of SSTs averaged

Model name	Hindcast ensemble size	Centre of origin
CMCC-SPS3	40	Centro Euro-Mediterraneo sui Cambiamenti Climatici (CMCC)
CMCC-SPS3.5	40	Centro Euro-Mediterraneo sui Cambiamenti Climatici (CMCC)
DWD-GCFS2.0	30	Deutscher Wetterdienst (DWD)
DWD-GCFS2.1	30	Deutscher Wetterdienst (DWD)
ECCC-CanCM4i	10	Environment and Climate Change Canada (ECCC)
ECCC-GEM-NEMO	10	Environment and Climate Change Canada (ECCC)
ECCC-GEM5-NEMO	10	Environment and Climate Change Canada (ECCC)
ECMWF-SEAS5	25	European Centre for Medium-Range Weather Forecasts (ECMWF)
JMA-CPS2	10	Japan Meteorological Agency (JMA)
JMA-CPS3	10	Japan Meteorological Agency (JMA)
MF-Sys6	25	Météo-France (MF)
MF-Sys7	25	Météo-France (MF)
MF-Sys8	25	Météo-France (MF)
NCEP-CFSv2	12	National Centers for Environmental Prediction (NCEP)
UKMO-GloSea5-GC2-LI	42	UK Met Office (UKMO)
UKMO-GloSea6	42	UK Met Office (UKMO)

Table 1: *Seasonal forecast models from the C3S archive analysed in this study. Full details for these models and the datasets are available from the C3S Climate Data Store (https://confluence.ecmwf.int/display/CKB/Description+of+the+C3S+seasonal+multi-system).*

over the Nino 3.4 index region (170°W-120°W, 5°S-5°N). ENSO winters are identified when SST anomalies are magnitude greater than 0.5°K relative to a moving 30-year averaged climatology. An additional requirement is that the SST anomaly must remain over the threshold for four consecutive rolling three-month seasons, one of which must be DJF. Over the extended ERA5 period a total of 19 El Niño winters and 18 La Niña winters are identified, and over the C3S period a total of 7 El Niño winters and 8 La Niña winters are identified. For the interannual correlations, the 3-month DJF winter Nino-3.4 SST index is used, calculated as detailed above from the HadISST dataset.

d. East Atlantic (EA) index

The East Atlantic (EA) index is defined here as the second EOF of the early winter (ND) area-weighted mean sea-level pressure (SLP) anomalies over the Euro-Atlantic sector (90°W-40°E, 20°-70°N). These are calculated using the ERA5 data to calculate the reference patterns and indices. The reference EOF patterns are shown in Figure S1. The C3S indices are calculated by projecting the SLP anomalies from each model onto the pattern of the EA from the ERA5 dataset and then renormalised. This is repeated for all of the C3S models to generate the hindcast EA indices.

e. Blocking event diagnostic

To assess the behaviour of atmospheric blocking we apply a two-dimensional large-scale wave-breaking index, which has been commonly used to identify blocking events in the literature (e.g. Woollings et al. 2008). Here we follow the methodology outlined in Masato et al. (2013). The blocking index uses daily averaged Z500 fields and identifies meridional reversals of the climatological equator-to-pole gradient, calculated over regions spanning 15 degrees to the north and south of each point in the northern midlatitudes. Events must also extend at least 15 degrees in longitude and are required to persist for at least 5 days to be identified as blocking events.

f. North Atlantic eddy-driven jet diagnostic

In the analysis below we analyse the behaviour of the daily North Atlantic eddy-driven jet, its variability and response to ENSO. To identify the latitude of the eddy-driven jet over the North Atlantic we broadly follow the method of (Woollings et al. 2010). The daily zonal wind in the lower troposphere (at 850 hPa) is zonally averaged between 0-60°W, retaining values from 15-75°N. The daily zonal mean zonal wind is then low-pass filtered using a 10-day Lanczos filter to identify changes in the jet on timescales longer than those of individual synoptic systems. The North Atlantic eddy-driven jet latitude is identified as the latitude of the maximum wind speed for each day. These daily jet latitudes are used to compute probability distributions of the jet latitude using a kernel density estimate, with standard bandwidth $h = 1.06\sigma n^{-1/5}$, where σ is the standard deviation and n is the sample size (Silverman 1981). In the pdfs presented below, we use the same h calculated from ERA5 to smooth the pdfs from the C3S simulations, which provides a fairer comparison between the reanalysis and model data.

g. Ratio of predictable components (RPC)

To quantify the signal-to-noise in the hindcasts we compute the ”ratio of predictable components” (RPC), which has previously been used in various studies evaluating forecast skill (e.g. Eade et al. 2014; Scaife and Smith 2018). The RPC is the ratio of the correlation skill between the ensemble mean hindcast and the observations (r_{mo}) and the correlation skill of the model ensemble mean predicting a single ensemble member (r_{mm}):

$$RPC = \frac{r_{mo}}{r_{mm}}. \tag{1}$$

To calculate r_{mm}, which can be referred to as a perfect model correlation, we remove one ensemble member from each season at random to create an individual realisation. The ensemble mean is calculated from the remaining ensemble members and correlated with the individual realisation. This is repeated 10000 times and the resulting r^2 values are averaged; the square-root of this average gives the perfect model correlation, r_{mm}.

3. Results

a. Overview of early winter hindcast skill and ENSO teleconnection in the C3S models

We begin our analysis of the early winter C3S model hindcasts be examining the ensemble mean correlation skill of hindcast SLP anomalies in each model, shown in Figure 1. As is typical for seasonal forecast systems, there is substantial correlation skill in the tropics and over much of the North Pacific. Over the extratropical North Atlantic, most of the models exhibit a local maximum in SLP correlation skill located somewhere to west of the British Isles and to the south of Greenland, though the precise position and magnitude of the maxima varies across models. These SLP skill maps are consistent with the results shown by Thornton et al. (2023) for the ensemble mean of a smaller subset of these C3S models, albeit for the sightly different NDJ season (here we analyse the ND early winter season as this is the season that demonstrates the strongest and most consist ENSO teleconnection; O'Reilly et al. *submitted to QJRMS*). The local maxima in SLP correlation skill in the eastern North Atlantic that are seen in the C3S models project onto the region most strongly associated with the EA pattern (i.e. Figure S1) and the early winter ENSO teleconnection.

To examine the representation of the early winter ENSO teleconnections in the C3S model hindcasts, along with the associated influence on the ensemble mean correlation skill, we now examine the SLP difference between El Niño and La Niña years; these are shown in Figure 2 for each C3S model and also for the ERA5 dataset. Correlations between the Nino-3.4 index and the SLP anomaly in each ensemble member are shown in contours. The C3S models all show some

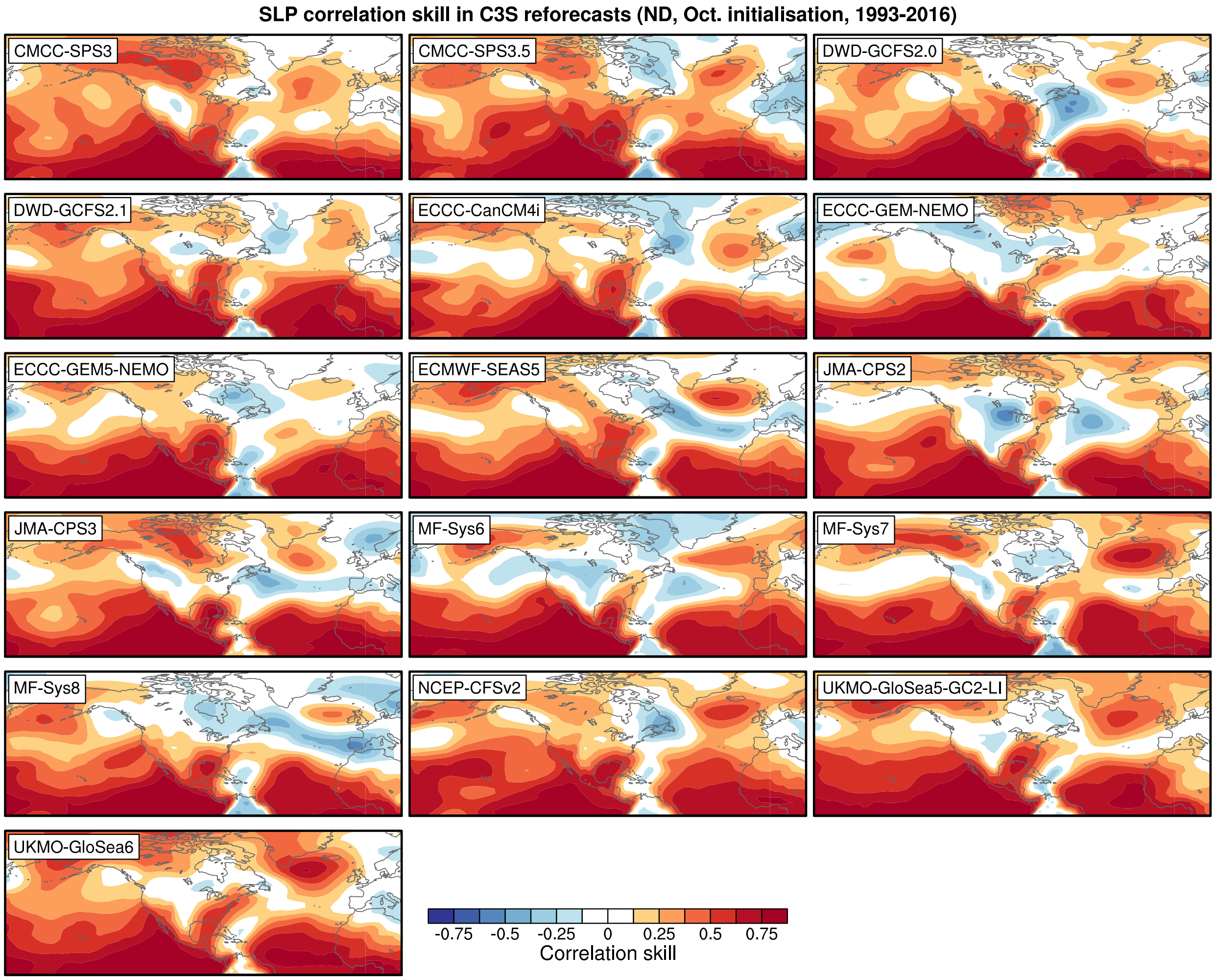

FIG. 1: *Ensemble mean hindcast correlation skill for early winter (ND) SLP in each of the C3S models over the period 1993-2016.*

form of negative SLP ENSO difference over the eastern North Atlantic, though showing some variation in the magnitude of the difference and the strength of the negative correlation between SLP and the the Nino-3.4 index. In all models, however, the ENSO teleconnection as measured by SLP is much weaker than that seen in ERA5. This is most clear for the C3S reference period (i.e. 1993-2016), though the models are also substantially weaker for the extended ERA5 period, which might be considered a statistically more robust measure of the observed teleconnection.

The weak early winter ENSO teleconnection to the North Atlantic is not only evident in the SLP anomaly. Figure 3 shows the C3S average teleconnection in terms of zonal wind anomalies, alongside the equivalent teleconnection estimated from ERA5. For both the upper-tropospheric

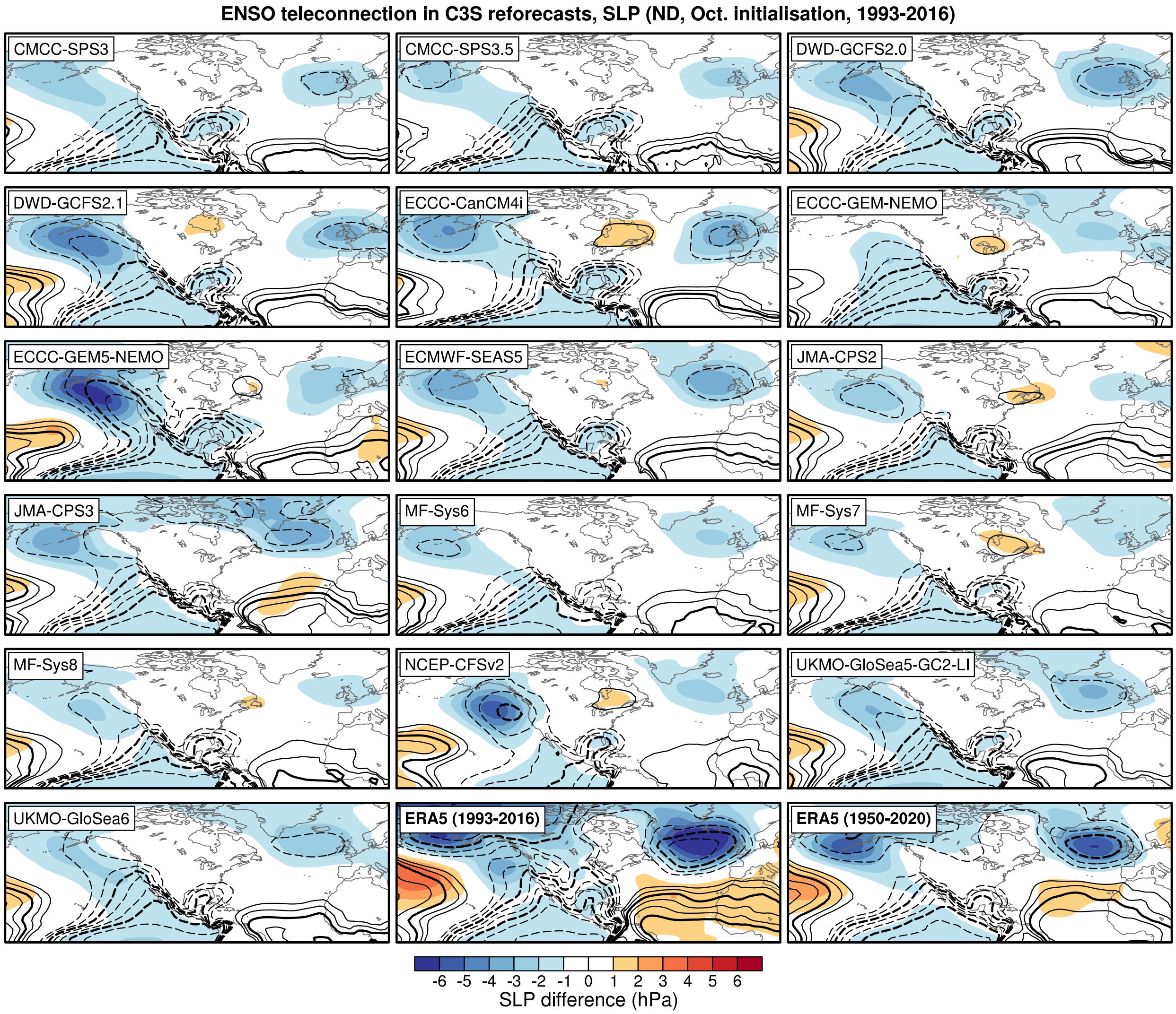

FIG. 2: *Early winter (ND) ENSO teleconnection calculated using SLP anomaly in each of the C3S models over the period 1993-2016. Shading shows the composite difference between El Nino and La Nina years (defined using the ONI index, see Methods) and the contours show the correlation between the SLP anomaly in each ensemble member and the observed Nino-3.4 SST index. Contours start from 0.2 with an interval of 0.1, and are emboldened at 0.4 and 0.7; negative contours are indicated by dashed lines. Also shown are the equivalent plots for the ERA5 data over an extended period (1950-2020).*

winds (U_{200}) and lower-tropospheric winds (U_{850}) it is clear that the influence of ENSO on the North Atlantic jet anomalies is weaker in the C3S models than in reanalysis. In terms of upper-level winds, it seems the disparities are most obvious in the North Atlantic, with the North Pacific

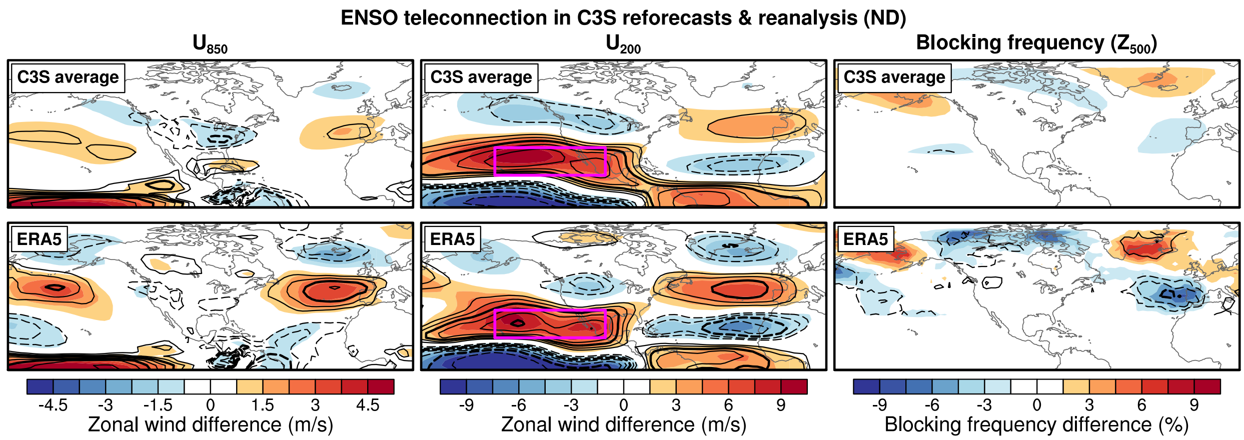

FIG. 3: *Early winter (ND) ENSO teleconnection averaged across the 16 different C3S models over the period 1993-2016, calculated for U_{850}, U_{200} and blocking frequency (see Methods). Shading shows the composite difference between El Nino and La Nina years (defined using the ONI index, see Methods) and the contours show the correlation between each variable anomaly in each ensemble member and the observed Nino-3.4 SST index. Contours start from 0.2 with an interval of 0.1, and are emboldened at 0.4 and 0.7; negative contours are indicated by dashed lines. Also shown are the equivalent plots for the ERA5 data over an extended period (1950-2020).*

teleconnection being of similar strength in the C3S models and the reanalysis, though there are some disparities in the lower-tropospheric winds. The ENSO impact on early winter blocking events is also shown in Figure 3. Previous observational analysis shows that the ENSO influence on the North Atlantic jet is established through changes in the frequency of poleward jet excursions and associated Iberian wave breaking events (O'Reilly et al., *submitted to QJRMS*), and this is evident in the blocking frequency shown in ERA5 here. In contrast, there are only very modest changes in the frequency of Iberian wave breaking events associated with ENSO in the C3S models. Together these provide a consistent picture of the dynamical changes over the North Atlantic in response to ENSO being substantially weaker in the C3S models than in observations.

b. Signal-to-noise of the East Atlantic index hindcasts and link to the ENSO teleconnection strength

To more quantitively compare the hindcast skill across the C3S models it is useful to analyse the skill of the East Atlantic (EA) index (see Methods). The EA index is a useful measure as it captures the main areas of skill over the North Atlantic during early winter and also dominates the ENSO teleconnection to the North Atlantic during this period. The ensemble mean hindcast

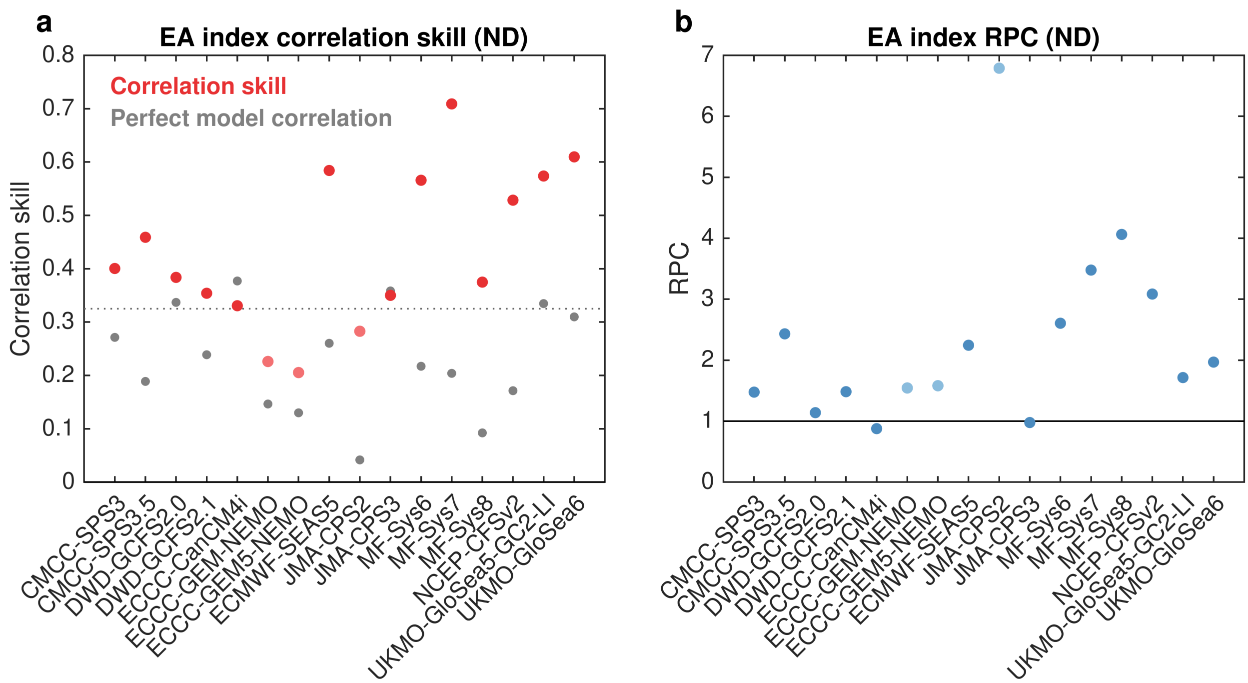

FIG. 4: ***a*** *Ensemble mean hindcast correlation skill (red circles) and the perfect model correlation skill (grey circles) for the EA index over the period 1993-2016 for each of the C3S models (the dotted line indicates the correlation skill corresponding to* $p = 0.05$ *based on a t-test).* ***b*** *Ratio of predictable components (RPC) for the EA index hindcasts for each of the C3S models (the solid line indicates where RPC*$= 1$*, which would indicate a reliable forecast by this measure and models with RPC*> 1 *being underconfident). Models that have hindcast correlation skills with p-values less than 0.05 are indicated by lighter shaded circles in both panels.*

correlation skill (i.e. r_{mo}) of the early winter EA index in the C3S models is shown in Figure 4a. Skill varies across the models but the vast majority of the models exhibit skill levels above $r = 0.3$, with only three of the models exhibiting correlation skills with $p > 0.05$ (based on a t-test). Also shown in Figure 4a is the perfect model correlation (i.e. r_{mm}) for each of the C3S models. For all but two of the models, the perfect model correlation is lower than the hindcast correlation skill and in some cases it is much lower. The signal-to-noise of the hindcast EA indices (in terms of RPC, see Methods) is shown in Figure 4b. The C3S models nearly all have $RPC > 1$, demonstrating that predictions of the early winter EA index are generally underconfident.

To examine how ENSO influences the early winter EA index we computed the the correlation between the early winter EA index and Nino-3.4 index across ensemble members for each C3S model, these are shown in Figure 5a along with the equivalent correlation in ERA5. The correlation values vary between $r = 0.1 - 0.4$ for the C3S models but these are all less than in ERA5. For the C3S period (1993-2016) the correlation in ERA5 is 0.57, this short period is subject to substantial sampling uncertainty but even over a longer and perhaps more robust period (1950-2020) the correlation between the EA index and Nino-3.4 is 0.44, higher than any C3S model. The weak influence of ENSO on the EA index in early winter is consistent with the weak teleconnection patterns shown in Figures 2 & 3.

We now compare the signal-to-noise in the predictions of the EA index, in terms of RPC, with the strength of the ENSO teleconnection to the EA index in early winter, shown in Figure 5b. Previous studies have highlighted that the RPC is a more useful measure of the signal-to-noise ratio in model predictions that exhibit significant levels of skill (Hardiman et al. 2022); following this convention we plot the models that have ensemble mean hindcast skill with $p < 0.05$ (see Figure 4), though the conclusions drawn from the analysis are not sensitive to this specific criteria. From the distribution of the points in Figure 5b it is clear that across the C3S models, those with weaker ENSO teleconnections generally have larger signal-to-noise errors, with a linear correlation of $r = -0.76$. These results indicate that the weak ENSO teleconnection across the models is responsible for causing the early winter signal-to-noise problem over the North Atlantic.

To provide some further insight into the relationship between the RPC and the ENSO teleconnection strength, we consider a toy model of the hindcasts, which we outline here. We first model the EA index in the observations as being linearly dependent on ENSO:

$$EA^*_{obs} = \beta_{obs} N^*_{34} + \epsilon_{obs}, \tag{2}$$

where EA^*_{obs} is the normalised EA index, N^*_{34} is the normalised observed Nino-3.4 index, β_{obs} is a dimensionless regression coefficient and ϵ_{obs} is a random residual term with a mean of zero. Similarly, we can model the (normalised) forecast ensemble mean EA index, EA^*_{em}, and the (normalised) forecast ensemble member EA indices, EA^*_{mem}, as:

$$\begin{aligned} EA^*_{em} &= \beta_{em} N^*_{34} + \epsilon_{em}, \\ EA^*_{mem} &= \beta_{mem} N^*_{34} + \epsilon_{mem}. \end{aligned} \tag{3}$$

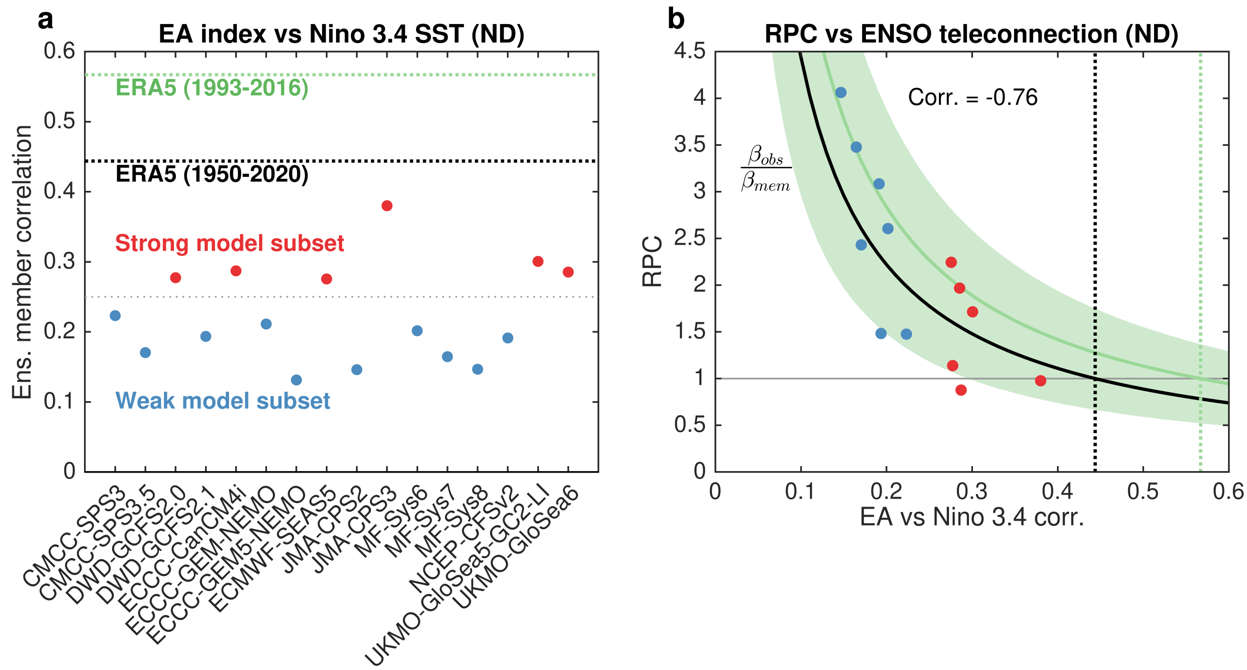

FIG. 5: ***a*** *Ensemble member correlation between the early winter EA index and the Nino 3.4 SST index for each of the C3S models (1993-2016). Also shown in thick dashed lines are the equivalent correlation for the early winter EA index calculated from reanalysis data for an extended period (1950-2020) and a shorter period that matches the C3S models (1993-2016). The models are separated into two subsets based on the strength of this correlation, with models greater than* $r = 0.25$ *corresponding to the "strong" subset (in red) and with models less than* $r = 0.25$ *corresponding to the "weak" subset (in blue).* ***b*** *Relationship between the ratio of predictable components (RPC) and the EA index vs. Nino 3.4 correlation (also equal to* β_{mem} *in the linear ENSO mode, see text). Curves of the scaling for a linear ENSO model,* $\frac{\beta_{obs}}{\beta_{mem}}$*, are also shown for values of* β_{obs} *from the ERA5 data over an extended period (1950-2020, in black) and a shorter period that matches the C3S models (1993-2016, in green)). The shading shows a 5-95% confidence interval for the green* $\frac{\beta_{obs}}{\beta_{mem}}$ *curve, estimated using a Monte Carlo resampling (random bootstrapping with replacement over years in the sample, repeated 10000 times).*

Note here that the normalised *observed* Nino-3.4 index, N_{34}^*, is included in the linear models as the seasonal forecasts of the Nino-3.4 index are very skillful over the lead-times considered here and this simplifies the expressions that follow (though does not materially affect the resulting scaling). Using the expressions for different normalised EA indices, we can now evaluate the correlations used to calculate the RPC:

$$\begin{aligned} r_{mo} &= corr(EA^*_{obs}, EA^*_{em}) = corr(\beta_{obs}N^*_{34} + \epsilon_{obs}, \beta_{em}N^*_{34} + \epsilon_{em}) \approx \beta_{obs}\beta_{em} \\ r_{mm} &= corr(EA^*_{mem}, EA^*_{em}) = corr(\beta_{mem}N^*_{34} + \epsilon_{mem}, \beta_{em}N^*_{34} + \epsilon_{em}) \approx \beta_{mem}\beta_{em}. \end{aligned} \tag{4}$$

Here we have assumed that the covariance between the residual terms is zero and that the residual terms average to zero. This results in a simple scaling of the RPC:

$$RPC = \frac{r_{mo}}{r_{mm}} \approx \frac{\beta_{obs}}{\beta_{mem}}. \tag{5}$$

Therefore, if this is an appropriate model, we should expect the RPC of the EA index hindcasts to be dependent on the ratio of the observed ENSO teleconnection strength (β_{obs}) and the ensemble member ENSO teleconnection strength (β_{mem}).

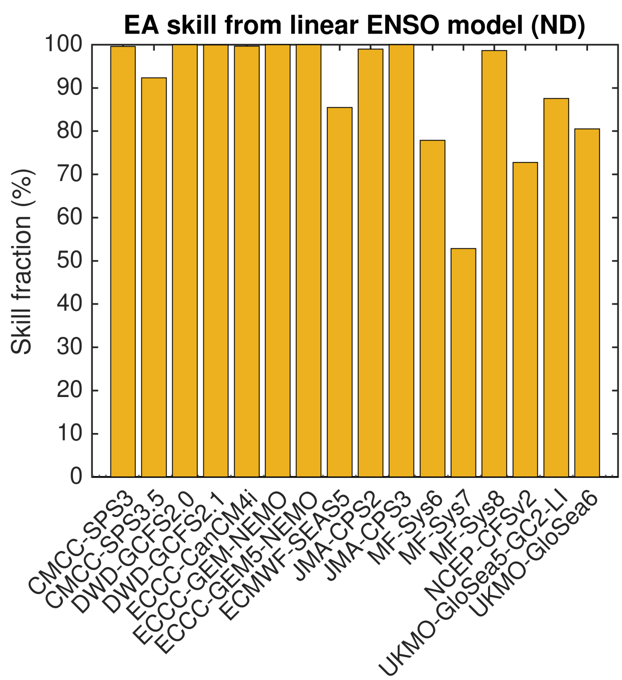

FIG. 6: *Fraction of EA index hindcast skill that can be accounted for by the linear ENSO model of the EA index for each C3S model, expressed here as a percentage.*

There are various assumptions that go into this toy model. An important assumption is that ENSO alone is responsible for the forecast skill in the EA index and that it does so in linear way. To test this assumption, we calculated the skill of a simple linear model fit to each hindcast model separately and compared this to the actual hindcast skill; the fraction of the actual hindcast skill (i.e. r_{mo}^2) that can be accounted for by the linear model is plotted in Figure 6. In all the C3S models, the majority of the skill can be recovered in the simple linear ENSO model, indicating that the linear model is a reasonable approach. It is important to note that the models that exhibit the highest hindcast correlation skill are those that cannot be fully explained by this linear model, which indicates some of the model skill arises from other, more complex, sources. A related assumption is that the residuals terms have zero covariance and zero mean (e.g. other sources of skill would result in a positive correlation between the residual terms). In reality, due to finite ensemble sizes and short hindcast periods these terms will not be exactly uncorrelated and any deviations from zero will deteriorate the fit of the scaling expression.

The predicted scaling of RPC for the early winter EA indices is plotted with the actual RPC values in Figure 5b. The green curve shows the RPC scaling for the observed ENSO teleconnection over the C3S period, along with shading that shows the sampling uncertainty. The RPC scaling from the toy model broadly captures the relationship between the actual RPC values calculated from the hindcasts and the actual ENSO teleconnection strength in the models (note that because the linear models are normalised, β_{mem} is equal to the correlation between the EA index and Nino-3.4 over ensemble members). In particular the scaling highlights the expected non-linearity of the RPC with respect to teleconnection strength, with consistent behaviour seen in the actual RPC values. The non-linear scaling of the RPC in terms of teleconnection strength also highlights a potential difficulty in using RPC to discriminate between models, as the expected RPC becomes more similar for models as their ENSO teleconnections approach the observed strength. These difficulties are of course exacerbated by the sampling uncertainties due to the short 24-year hindcast period.

In this section we have shown that the C3S models have robust but varying hindcast skill for the early winter EA index. However, the signals in the hindcasts, as measured by the perfect model correlation (r_{mm}), are generally too weak in the models, resulting in substantial signal-to-noise errors (i.e. Figure 4). The ENSO teleconnection to the EA index is too weak in all the hindcasts but shows substantial variability across the C3S models. Further analysis shows that models with a weaker teleconnection generally exhibit a larger RPC values and, therefore, a clearer signal-to-noise errors. Finally, we demonstrated that a toy model of the ENSO teleconnection to the early winter EA index can broadly explain the magnitude and RPC scaling across the models, depending only on the model teleconnection strength.

c. Exploring causes of the weak ENSO teleconnection in the C3S models

In the previous sections we have shown that the weak ENSO teleconnection is largely responsible for the of the signal-to-noise errors observed in the early winter hindcasts. We now turn our attention to the causes of this weak ENSO teleconnection to the North Atlantic in the early winter.

To begin, it is useful to revisit the mechanisms through which ENSO influences the North Atlantic circulation during the early winter. In a recent paper, O'Reilly et al. (*submitted to QJRMS*) showed that the ENSO teleconnection to the North Atlantic is largely through the modification of the poleward jet excursions, which project onto the EA pattern. The response of the North Atlantic jet is sensitive, on both subseasonal as well as seasonal timescales, to the jet and storm track anomalies over the eastern North Pacific. A schematic view of this is shown in the simple causal chain diagram in Figure 7a (following, e.g., Kretschmer et al. (2021)). Such a simple model is likely an oversimplification but explicitly stating the causal chain in this way allows us interrogate each step in this relationship in the models as well as reanalysis, and identify any key differences. We define normalised indices for ENSO, the Pacific Jet and the EA pattern and use linear regression between these indices to calculate the strength of these connections in each C3S model and in ERA5, shown in Figure 7b.

The C3S models all exhibit strong relationships between ENSO and the Pacific Jet (green points), which are all very similar to the value calculated from ERA5 data. However, the link between the Pacific Jet and the early winter EA index is much more variable across the C3S models (brown points), though all models are substantially weaker than the link between the Pacific Jet and EA index calculated from ERA5 data. This simple analysis suggests that the biggest differences in the total ENSO teleconnection pathway stems from the deficiencies in the response of the North Atlantic circulation to upstream circulation anomalies over the North Pacific. This conclusion is supported by the average C3S U200 teleconnection maps, shown in Figure 3, which show similar anomalies to ERA5 over the North Pacific but much weaker responses over the North Atlantic. These results indicate that differences in the ENSO teleconnection originate from differences in

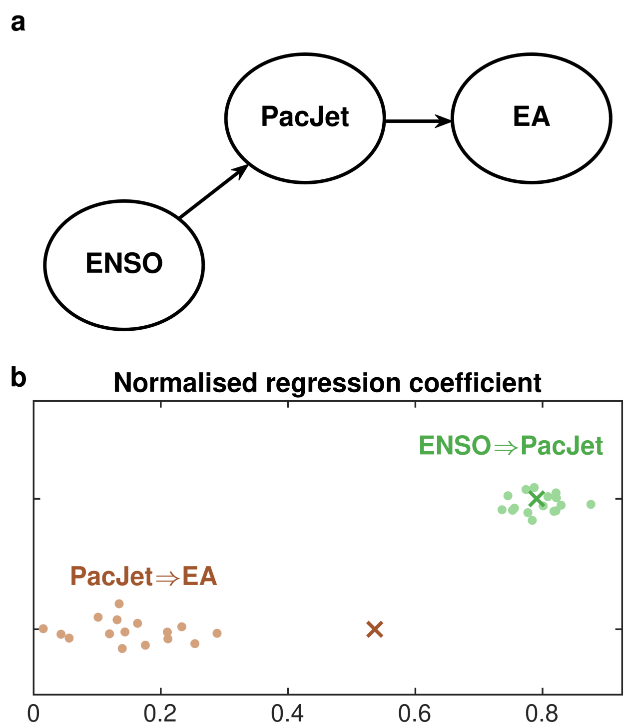

FIG. 7: ***a** Schematic of the causal chain (following, e.g., Kretschmer et al. (2021)) linking ENSO variability to the EA index variability over the North Atlantic (based on O'Reilly et al., submitted to QJRMS). Here "ENSO" refers specifically to the normalised Nino 3.4 SST index, "PacJet" refers to an index for the Pacific Jet defined as the normalised U_{200} anomaly averaged over the eastern North Pacific (shown by box in Figure 3) and "EA" refers to the normalised EA index. **b** The circles show the linear regression coefficients between the indices in the causal chain for each C3S model and the crosses indicate the coefficients calculated from the ERA5 dataset (1950-2020). A jitter has been added to the y-axis to aid visualisation of the individual points.*

the behaviour of the North Atlantic jet across the C3S models and prompt us to explore the North Atlantic jet in the models in more detail.

To explore the causes for the differences in ENSO teleconnection strength over the North Atlantic, we define two C3S model subsets based on the strength of the correlation between the EA index and the Nino-3.4 index across all ensemble members (shown in Figure 5a). The threshold was set at $\beta_{mem} = 0.25$, since from visual inspection (of Figure 5a) this provided the clearest separation of the models; this threshold results in six models in the "strong" model subset and ten models in the "weak" model subset. To examine the differences in model behaviour we first examine the climatologies of the zonal wind in the C3S models; the differences between the strong and weak subsets and the average C3S model bias with respect to ERA5 are shown in Figure 8.

There are some clear differences between the strong and weak model subsets over the North Atlantic, with the stronger models having stronger zonal winds over the northern part of the basin (Figure 8a,c). Over the North Atlantic, the jet is generally too far south in the C3S models with significantly weaker winds over the northern part of the basin (Figure 8b,d). The strong subset of models, therefore, have reduced biases over a northern band of the North Atlantic basin (i.e. between the southern tip of Greenland and Scotland). The weak subset generally have stronger winds further south in the North Atlantic. There are also substantial difference in the jets upstream over the North Pacific, suggesting that biases here may be linked to the North Atlantic biases. Together, these results support the intuitive conclusion that a better model representation of climatological North Atlantic jet behaviour improves the fidelity of the early winter ENSO teleconnection.

In addition to analysing the climatological circulation, it also useful to examine the representation of sub-seasonal circulation variability in the C3S models. The early winter ENSO teleconnection is linked to changes in blocking frequency near the Iberian peninsula (i.e. Figure 3). Differences in climatological blocking frequency between the strong and weak subsets, and the average C3S model blocking bias are shown in Figure 8e & 8f. A major difference between the strong and weak models is found over western North America and southern Greenland, with significantly more blocking occurring in the weak subset. On average, the C3S models exhibit too much blocking over this region, with the stronger subset of models demonstrating better agreement with observations compared to the weaker models. Blocking events over this southern Greenland region are typically associated with southward shifts in the jet (e.g. Woollings et al. 2010), so the higher blocking frequency in weaker subsets of models is consistent with the stronger jets over the southern part of the North Atlantic basin in these models (i.e. Figure 8a). The C3S models generally have too little blocking over the Iberian region, where there is a clear ENSO influence in observations (i.e. Figure 3), though this seems to plague both the strong and weak models equally, with the variation in ENSO teleconnection strength across the models demonstrating more sensitivity to the climatological Greenland blocking frequency.

To further examine the differences in model North Atlantic jet behaviour, we now analyse distributions of the daily North Atlantic eddy-driven jet latitude (see Methods); the jet latitude distributions

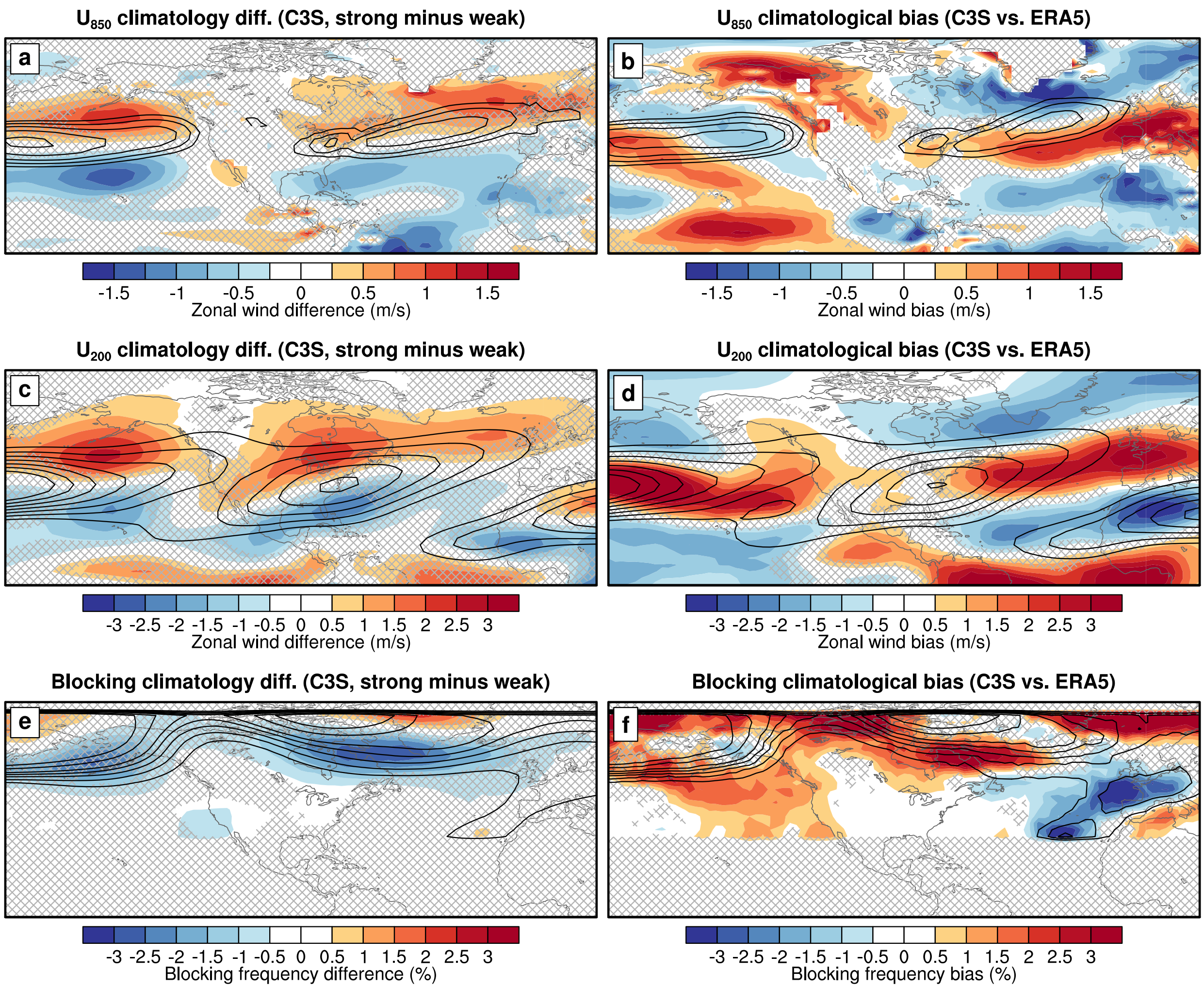

FIG. 8: ***a*** *The composite U_{850} difference between the climatologies of the strong and weak subsets of C3S models (as defined in the text and Figure 6a). The C3S average climatology is shown in black contours every 1 m/s from 7m/s.* ***b*** *The C3S average climatological U_{850} bias with respect to ERA5 (defined C3S minus ERA5). The ERA5 climatology (1950-2020) is shown in black contours every 1 m/s from 7m/s.* ***c***,***d*** *as in* ***a***,***b*** *but for U_{200}; climatology is shown in black contours every 5 m/s from 20m/s.* ***e***,***f*** *as in* ***a***,***b*** *but for blocking frequency (see Methods); climatology is shown in black contours at 5%, 7.5%, 10%, 12.5%, 15%, 20% and 25%. Hatching shows where the 5-95% confidence interval of the difference/bias does not cross zero; the confidence intervals are estimated using a Monte Carlo resampling (random bootstrapping with replacement, repeated 10000 times).*

are shown for the C3S models and ERA5 in Figure 9a. The C3S models clearly underestimate the frequency of the poleward jet excursions, around 55-60°N, and generally overestimate the jet frequency further south. The strong model subset exhibits higher frequencies of poleward jet

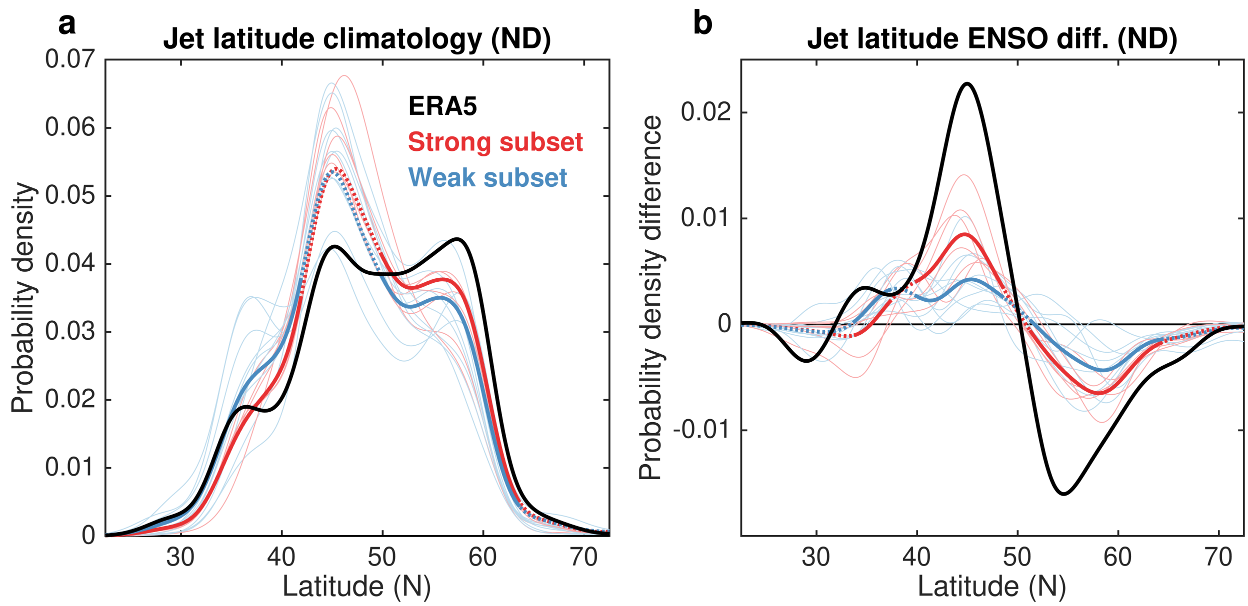

FIG. 9: ***a*** *Climatological eddy-driven jet latitude pdfs (see Methods) shown for each individual C3S model in light coloured lines and for ERA5 in black. The average of these pdfs for the strong and weak subsets of models are shown in the thick red and blues lines, respectively.* ***b*** *as in* ***a*** *but for the difference in eddy-driven jet latitude pdfs between El Niño and La Niña years. The dotted thick red/blue lines shows where the 5-95% confidence interval of the difference between the strong and weak subsets does not cross zero; the confidence intervals are estimated using a Monte Carlo resampling (random bootstrapping with replacement, repeated 10000 times).*

excursions on average and their behaviour it closer to that seen in the reanalysis, compared to the weak model subset. The weak model subset tends to more strongly overestimate the southern jet frequency, around 35-40°N, compared to the strong model subset. These southern jet events are often associated with Greenland blocking events (Woollings et al. 2010) so this jet variability is consistent with the high Greenland blocking frequency seen in the weak model subset (i.e. Figure 8e). A major feature of the jet distribution is that the frequency of the central peak is far too high in the vast majority of the models; this is likely closely related to the lack of blocking events over the Iberian region, which are associated with more frequent poleward jet events and lower frequencies in the central position (Woollings et al. 2010).

A consistent picture that emerges from the analysis of the jet latitude distributions is that models with a better representation of the poleward jet events generally have stronger early winter ENSO teleconnections. To demonstrate this more clearly we have plotted the difference between the jet latitude between El Niño and La Niña years (in Figure 9b). The ENSO teleconnection in observations is strongly connected to changes in the occurrence of poleward jet excursions, which occur more frequently in La Niña years. The C3S models that struggle to simulate these events often enough in the climatology (i.e. Figure 9a) tend to be those models that show a smaller jet latitude frequency difference in response to ENSO and therefore show a weaker ENSO teleconnection.

In this section we have demonstrated that, across the C3S models, the strength of the ENSO teleconnection is linked to the climatological behaviour of North Atlantic jet. Models that have a stronger ENSO teleconnection tend to have stronger jets over the northern part of the North Atlantic basin, associated with an increased frequency of poleward jet excursions. The models that have a weaker ENSO teleconnection tend to exhibit more blocking over southern Greenland, which is associated with the jet being shifted further south and less poleward jet excursions. We showed in the previous section that the weak ENSO teleconnection is a clear source of signal-to-noise errors in the early winter hindcasts. The results here show that systematic biases in the climatological behaviour of the North Atlantic jet are contributing to the weak teleconnection and associated signal-to-noise errors in the C3S models.

4. Discussion

In this study we have examined early winter Euro-Atlantic predictability in an ensemble of state-of-the-art seasonal forecasting systems. The majority of the models analysed show skill in the hindcasts of the extratropical large-scale atmospheric circulation in early winter, which mostly projects onto the EA pattern. The predictability is strongly tied to the ENSO teleconnection to the North Atlantic, which is skillfully captured but the teleconnection is typically too weak in the models. The model hindcasts of the EA index generally exhibit a substantial signal-to-noise error, with the model signal being lower than would be expected for the demonstrated level of hindcast skill (i.e. $RPC > 1$), though there is a variation in this error across models. The signal-to-noise error is strongly dependent on the strength of the ENSO teleconnection in the models, with models that exhibit a weaker teleconnection displaying a larger signal-to-noise problem. The dependency on ENSO teleconnection strength can be explained using a scaling relationship derived from a toy model. Further analysis reveals that the strength of the ENSO teleconnection in the model is linked to climatological biases in the behaviour of the North Atlantic jet. Models that better represent the dynamics of the jet over the northern part of the basin, with more frequent poleward jet excursions and less frequent Greenland blocking events, are typically better at representing the strength of the ENSO teleconnection to the North Atlantic in early winter, with lower associated signal-to-noise errors.

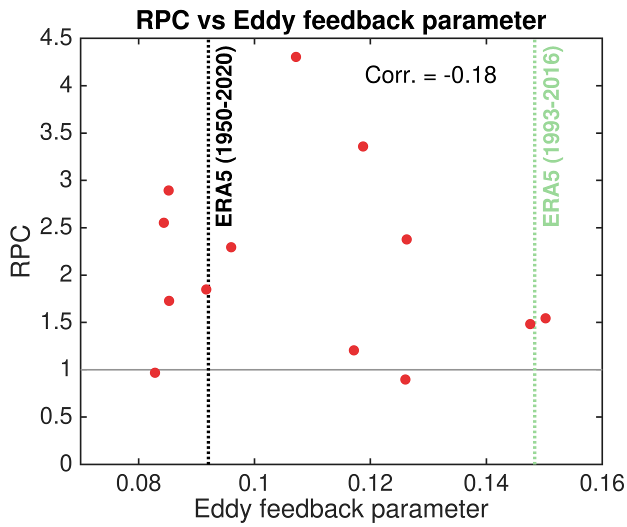

FIG. 10: *Ratio of predictable components (RCP) for the early winter (ND) EA index hindcasts from the C3S models plotted against the eddy feedback parameter defined in Hardiman et al. (2019) (and following (Smith et al. 2022)). Specifically, the eddy feedback parameter is calculated as the area-weighted average of* $corr(\overline{u}, \nabla \cdot \boldsymbol{F_H})^2$ *between 20-72°N (calculated at 500 hPa), where* $\boldsymbol{F_H}$ *is the horizontal quasigeostrophic Eliassen-Palm flux,* $\overline{u}$ *is the zonal mean zonal wind and the correlation is calculated on seasonally averaged data. Also shown are the values of the eddy feedback parameter from the ERA5 dataset, calculated over both the C3S period and an extended period. The models are the same as those plotted in Figure 5b. The full latitudinal variation of the correlation term,* $corr(\overline{u}, \nabla \cdot \boldsymbol{F_H})$*, also shows very good agreement across the models and ERA5 (Figure S2).*

Our analysis has highlighted the weak ENSO teleconnection, as well as associated biases in the behaviour of the North Atlantic jet, as the cause of many of the signal-to-noise errors seen in the early winter hindcasts. It is worthwhile comparing how these findings fit with previous theories on the origins of signal-to-noise errors. One prominent theory, proposed in Scaife et al. (2019) and further investigated in Hardiman et al. (2022), is that deficiencies in the eddy feedbacks are responsible for the weak predictable signal in models. Hardiman et al. (2022) showed that, for winter (DJF) seasonal hindcasts of the Arctic Oscillation and North Atlantic Oscillation indices, the RPC is correlated with an "eddy feedback parameter", which is a measure of the feedback of the horizontal Eliassen-Palm flux on the zonal mean jet (following Smith et al. (2022); see caption of Figure 10 for specific definition). To examine how well this explains the signal-to-noise errors in the early winter EA index hindcasts, we computed the eddy feedback parameter and compared it with the RPC (shown in Figure 10). Overall, the eddy feedback parameter for the C3S models analysed in this study is very similar to the ERA5 values and, moreover, the variation in the eddy feedback parameter is not strongly related to the RPC. The correlation between the eddy feedback parameter and RPC is $r = -0.18$, which is very small compared to the correlation between the ENSO teleconnection strength and RPC, $r = -0.76$ (i.e. Figure 5b).

Although we find the eddy feedback parameter to not be be a useful indicator of the signal-to-noise error in these early winter hindcasts, this does not mean that deficiencies in eddy feedbacks are not playing a role. Transient eddy feedbacks are crucial in shaping blocking events and shifts in the North Atlantic jet, and these are important in determining the early winter ENSO teleconnection in observations (O'Reilly et al., *submitted to QJRMS*). In the analysis above, we found that biases in the eddy-driven jet latitude distributions underly the weak ENSO teleconnections, which does broadly represent a deficiency in eddy feedbacks. However, it could be more useful to consider the signal-to-noise errors to stem from the systematic biases in the representation of the North Atlantic jet - this will not necessarily directly relate to a zonally averaged measure of eddy feedback, as seen here for the eddy feedback parameter. The biases in the jet latitude distributions of the C3S models here also exhibit some consistencies with the regime hypothesis of Strommen and Palmer (2019), where here the frequency of the poleward jet events, or regimes, are systematically underestimated by the models and display a muted change in frequency to predictable ENSO forcing (e.g. Figure 9b).

Beyond this study, the approach applied here could provide a useful framework for exploring the origins of signal-to-noise errors in other seasons, regions and over different timescales. Specifically, the general process of identifying important predictable drivers of large-scale circulation anomalies and exploring how biases in the model behaviour are undermining the predictable model signals. Here, the dominance of the ENSO signal in early winter allowed for a relatively clear understanding of the processes driving the weak model signals but things may not be as clear in other instances. For example, using a similar approach to study the predictable signals of the later winter NAO would be more complex because there are multiple important drivers (e.g. Folland et al. 2012; Dunstone et al. 2016) and model skill levels are typically not as high (e.g. Hardiman et al. 2022). Nonetheless, applying this process and identifying biases in the model behaviour that are linked to the weak predictable signals provides a practical approach towards developing further understanding of other signal-to-noise errors in coupled climate models.

Acknowledgements

COR was supported by a Royal Society University Research Fellowship (URF\R1\201230).

Data availability statement

The data used in this paper are all open access datasets available on public servers.

References

Ayarzagüena, B., S. Ineson, N. J. Dunstone, M. P. Baldwin, and A. A. Scaife, 2018: Intraseasonal Effects of El Niño–Southern Oscillation on North Atlantic Climate. *Journal of Climate*, **31 (21)**, 8861–8873, https://doi.org/10.1175/JCLI-D-18-0097.1, URL https://journals.ametsoc.org/view/journals/clim/31/21/jcli-d-18-0097.1.xml, publisher: American Meteorological Society Section: Journal of Climate.

Baker, L. H., L. C. Shaffrey, R. T. Sutton, A. Weisheimer, and A. A. Scaife, 2018: An Intercomparison of Skill and Overconfidence/Underconfidence of the Wintertime North Atlantic Oscillation in Multimodel Seasonal Forecasts. *Geophysical Research Letters*, **45 (15)**, 7808–7817, https://doi.org/10.1029/2018GL078838, URL https://onlinelibrary.wiley.com/doi/abs/10.1029/2018GL078838, _eprint: https://onlinelibrary.wiley.com/doi/pdf/10.1029/2018GL078838.

Bracegirdle, T. J., H. Lu, R. Eade, and T. Woollings, 2018: Do CMIP5 Models Reproduce Observed Low-Frequency North Atlantic Jet Variability? *Geophysical Research Letters*, **45 (14)**, 7204–7212, https://doi.org/10.1029/2018GL078965, URL https://onlinelibrary.wiley.com/doi/abs/10.1029/2018GL078965, _eprint: https://onlinelibrary.wiley.com/doi/pdf/10.1029/2018GL078965.

Charlton-Perez, A. J., J. Bröcker, T. N. Stockdale, and S. Johnson, 2019: When and where do ECMWF seasonal forecast systems exhibit anomalously low signal-to-noise ratio? *Quarterly Journal of the Royal Meteorological Society*, **145 (725)**, 3466–3478, https://doi.org/10.1002/qj.3631, URL https://onlinelibrary.wiley.com/doi/abs/10.1002/qj.3631, _eprint: https://onlinelibrary.wiley.com/doi/pdf/10.1002/qj.3631.

Clark, R. T., P. E. Bett, H. E. Thornton, and A. A. Scaife, 2017: Skilful seasonal predictions for the European energy industry. *Environmental Research Letters*, **12 (2)**, 024 002, https://doi.org/10.1088/1748-9326/aa57ab, URL https://dx.doi.org/10.1088/1748-9326/aa57ab, publisher: IOP Publishing.

Dunstone, N., D. Smith, A. Scaife, L. Hermanson, R. Eade, N. Robinson, M. Andrews, and J. Knight, 2016: Skilful predictions of the winter North Atlantic Oscillation one year ahead. *Nature Geoscience*, **9 (11)**, 809–814, https://doi.org/10.1038/ngeo2824, URL https://www.nature.com/articles/ngeo2824, number: 11 Publisher: Nature Publishing Group.

Dunstone, N., and Coauthors, 2018: Skilful Seasonal Predictions of Summer European Rainfall. *Geophysical Research Letters*, **45 (7)**, 3246–3254, https://doi.org/10.1002/2017GL076337, URL https://onlinelibrary.wiley.com/doi/abs/10.1002/2017GL076337, _eprint: https://onlinelibrary.wiley.com/doi/pdf/10.1002/2017GL076337.

Dunstone, N., and Coauthors, 2023: Skilful predictions of the Summer North Atlantic Oscillation. *Communications Earth & Environment*, **4 (1)**, 1–11, https://doi.org/10.1038/s43247-023-01063-2, URL https://www.nature.com/articles/s43247-023-01063-2, number: 1 Publisher: Nature Publishing Group.

Eade, R., D. Smith, A. Scaife, E. Wallace, N. Dunstone, L. Hermanson, and N. Robinson, 2014: Do seasonal-to-decadal climate predictions underestimate the predictability of the real world? *Geophysical Research Letters*, **41 (15)**, 5620–5628, https://doi.org/10.1002/2014GL061146, URL https://onlinelibrary.wiley.com/doi/abs/10.1002/2014GL061146, _eprint: https://onlinelibrary.wiley.com/doi/pdf/10.1002/2014GL061146.

Folland, C. K., A. A. Scaife, J. Lindesay, and D. B. Stephenson, 2012: How potentially predictable is northern European winter climate a season ahead? *International Journal of Climatology*, **32 (6)**, 801–818, https://doi.org/10.1002/joc.2314, URL https://onlinelibrary.wiley.com/doi/abs/10.1002/joc.2314, _eprint: https://onlinelibrary.wiley.com/doi/pdf/10.1002/joc.2314.

Garfinkel, C. I., W. Chen, Y. Li, C. Schwartz, P. Yadav, and D. Domeisen, 2022: The Winter North Pacific Teleconnection in Response to ENSO and the MJO in Operational Subseasonal Forecasting Models Is Too Weak. *Journal of Climate*, **35 (24)**, 8013–8030, https://doi.org/10.1175/JCLI-D-22-0179.1, URL https://journals.ametsoc.org/view/journals/clim/35/24/JCLI-D-22-0179.1.xml, publisher: American Meteorological Society Section: Journal of Climate.

Hardiman, S. C., N. J. Dunstone, A. A. Scaife, D. M. Smith, R. Comer, Y. Nie, and H.-L. Ren, 2022: Missing eddy feedback may explain weak signal-to-noise ratios in climate predictions. *npj Climate and Atmospheric Science*, **5 (1)**, 1–8, https://doi.org/10.1038/s41612-022-00280-4, URL https://www.nature.com/articles/s41612-022-00280-4, number: 1 Publisher: Nature Publishing Group.

Hardiman, S. C., N. J. Dunstone, A. A. Scaife, D. M. Smith, S. Ineson, J. Lim, and D. Fereday, 2019: The Impact of Strong El Niño and La Niña Events on the North Atlantic. *Geophysical Research Letters*, **46 (5)**, 2874–2883, https://doi.org/10.1029/2018GL081776, URL https://onlinelibrary.wiley.com/doi/abs/10.1029/2018GL081776, _eprint: https://onlinelibrary.wiley.com/doi/pdf/10.1029/2018GL081776.

Hersbach, H., and Coauthors, 2020: The ERA5 global reanalysis. *Quarterly Journal of the Royal Meteorological Society*, **146 (730)**, 1999–2049, https://doi.org/10.1002/qj.3803, URL https://onlinelibrary.wiley.com/doi/abs/10.1002/qj.3803, _eprint: https://onlinelibrary.wiley.com/doi/pdf/10.1002/qj.3803.

Hurrell, J. W., Y. Kushnir, G. Ottersen, and M. Visbeck, 2003: An Overview of the North Atlantic Oscillation. *The North Atlantic Oscillation: Climatic Significance and Environmental Impact*, American Geophysical Union (AGU), 1–35, https://doi.org/10.1029/134GM01, URL https://onlinelibrary.wiley.com/doi/abs/10.1029/134GM01, _eprint: https://onlinelibrary.wiley.com/doi/pdf/10.1029/134GM01.

Johansson, , 2007: Prediction Skill of the NAO and PNA from Daily to Seasonal Time Scales. *Journal of Climate*, **20 (10)**, 1957–1975, https://doi.org/10.1175/JCLI4072.1, URL https://journals.ametsoc.org/view/journals/clim/20/10/jcli4072.1.xml, publisher: American Meteorological Society Section: Journal of Climate.

King, M. P., I. Herceg-Bulić, I. Bladé, J. García-Serrano, N. Keenlyside, F. Kucharski, C. Li, and S. Sobolowski, 2018: Importance of Late Fall ENSO Teleconnection in the Euro-Atlantic Sector. *Bulletin of the American Meteorological Society*, **99 (7)**, 1337–1343, https://doi.org/10.1175/BAMS-D-17-0020.1, URL https://journals.ametsoc.org/view/journals/bams/99/7/bams-d-17-0020.1.xml, publisher: American Meteorological Society Section: Bulletin of the American Meteorological Society.

Kretschmer, M., S. V. Adams, A. Arribas, R. Prudden, N. Robinson, E. Saggioro, and T. G. Shepherd, 2021: Quantifying Causal Pathways of Teleconnections. *Bulletin of the American Meteorological Society*, **102 (12)**, E2247–E2263, https://doi.org/10.1175/BAMS-D-20-0117.1, URL https://journals.ametsoc.org/view/journals/bams/102/12/BAMS-D-20-0117.1.xml, publisher: American Meteorological Society Section: Bulletin of the American Meteorological Society.

Marcheggiani, A., J. Robson, P.-A. Monerie, T. J. Bracegirdle, and D. Smith, 2023: Decadal Predictability of the North Atlantic Eddy-Driven Jet in Winter. *Geophysical Research Letters*, **50 (8)**, e2022GL102 071, https://doi.org/10.1029/2022GL102071, URL https://onlinelibrary.wiley.com/doi/abs/10.1029/2022GL102071, _eprint: https://onlinelibrary.wiley.com/doi/pdf/10.1029/2022GL102071.

Masato, G., B. J. Hoskins, and T. Woollings, 2013: Wave-Breaking Characteristics of Northern Hemisphere Winter Blocking: A Two-Dimensional Approach. *Journal of Climate*, **26 (13)**, 4535–4549, https://doi.org/10.1175/JCLI-D-12-00240.1, URL https://journals.ametsoc.org/view/journals/clim/26/13/jcli-d-12-00240.1.xml, publisher: American Meteorological Society Section: Journal of Climate.

Molteni, F., and A. Brookshaw, 2023: Early- and late-winter ENSO teleconnections to the Euro-Atlantic region in state-of-the-art seasonal forecasting systems. *Climate Dynamics*, https://doi.org/10.1007/s00382-023-06698-7, URL https://doi.org/10.1007/s00382-023-06698-7.

O'Reilly, C. H., A. Weisheimer, T. Woollings, L. J. Gray, and D. MacLeod, 2019: The importance of stratospheric initial conditions for winter North Atlantic Oscillation predictability and implications for the signal-to-noise paradox. *Quarterly Journal of the Royal Meteorological Society*, **145 (718)**, 131–146, https://doi.org/10.1002/qj.3413, URL https://onlinelibrary.wiley.com/doi/abs/10.1002/qj.3413, _eprint: https://onlinelibrary.wiley.com/doi/pdf/10.1002/qj.3413.

Ossó, A., R. Sutton, L. Shaffrey, and B. Dong, 2020: Development, Amplification, and Decay of Atlantic/European Summer Weather Patterns Linked to Spring North Atlantic Sea Surface Temperatures. *Journal of Climate*, **33 (14)**, 5939–5951, https://doi.org/10.1175/JCLI-D-19-0613.1, URL https://journals.ametsoc.org/view/journals/clim/33/14/JCLI-D-19-0613.1.xml, publisher: American Meteorological Society Section: Journal of Climate.

O'Reilly, C. H., D. J. Befort, A. Weisheimer, T. Woollings, A. Ballinger, and G. Hegerl, 2021: Projections of northern hemisphere extratropical climate underestimate internal variability and associated uncertainty. *Communications Earth & Environment*, **2 (1)**, 1–9, https://doi.org/10.1038/s43247-021-00268-7, URL https://www.nature.com/articles/s43247-021-00268-7, number: 1 Publisher: Nature Publishing Group.

O'Reilly, C. H., L. Zanna, and T. Woollings, 2019: Assessing External and Internal Sources of Atlantic Multidecadal Variability Using Models, Proxy Data, and Early Instrumental Indices. *Journal of Climate*, **32 (22)**, 7727–7745, https://doi.org/10.1175/JCLI-D-19-0177.1, URL https://journals.ametsoc.org/view/journals/clim/32/22/jcli-d-19-0177.1.xml, publisher: American Meteorological Society Section: Journal of Climate.

Rayner, N. A., D. E. Parker, E. B. Horton, C. K. Folland, L. V. Alexander, D. P. Rowell, E. C. Kent, and A. Kaplan, 2003: Global analyses of sea surface temperature, sea ice, and night marine air temperature since the late nineteenth century. *Journal of Geophysical Research: Atmospheres*, **108 (D14)**, https://doi.org/10.1029/2002JD002670, URL https://onlinelibrary.wiley.com/doi/abs/10.1029/2002JD002670, _eprint: https://onlinelibrary.wiley.com/doi/pdf/10.1029/2002JD002670.

Scaife, A. A., and D. Smith, 2018: A signal-to-noise paradox in climate science. *npj Climate and Atmospheric Science*, **1 (1)**, 1–8, https://doi.org/10.1038/s41612-018-0038-4, URL https://www.nature.com/articles/s41612-018-0038-4, number: 1 Publisher: Nature Publishing Group.

Scaife, A. A., and Coauthors, 2014: Skillful long-range prediction of European and North American winters. *Geophysical Research Letters*, **41 (7)**, 2514–2519, https://doi.org/10.1002/2014GL059637, URL https://onlinelibrary.wiley.com/doi/abs/10.1002/2014GL059637, _eprint: https://onlinelibrary.wiley.com/doi/pdf/10.1002/2014GL059637.

Scaife, A. A., and Coauthors, 2019: Does increased atmospheric resolution improve seasonal climate predictions? *Atmospheric Science Letters*, **20 (8)**, e922, https://doi.org/10.1002/asl.922, URL https://onlinelibrary.wiley.com/doi/abs/10.1002/asl.922, _eprint: https://onlinelibrary.wiley.com/doi/pdf/10.1002/asl.922.

Silverman, B. W., 1981: Using Kernel Density Estimates to Investigate Multimodality. *Journal of the Royal Statistical Society: Series B (Methodological)*, **43 (1)**, 97–99, https://doi.org/10.1111/j.2517-6161.1981.tb01155.x, URL https://onlinelibrary.wiley.com/doi/abs/10.1111/j.2517-6161.1981.tb01155.x, _eprint: https://onlinelibrary.wiley.com/doi/pdf/10.1111/j.2517-6161.1981.tb01155.x.

Simpson, I. R., C. Deser, K. A. McKinnon, and E. A. Barnes, 2018: Modeled and Observed Multidecadal Variability in the North Atlantic Jet Stream and Its Connection to Sea Surface Temperatures. *Journal of Climate*, **31 (20)**, 8313–8338, https://doi.org/10.1175/JCLI-D-18-0168.1, URL https://journals.ametsoc.org/view/journals/clim/31/20/jcli-d-18-0168.1.xml, publisher: American Meteorological Society Section: Journal of Climate.

Smith, D. M., A. A. Scaife, and B. P. Kirtman, 2012: What is the current state of scientific knowledge with regard to seasonal and decadal forecasting? *Environmental Research Letters*, **7 (1)**, 015 602, https://doi.org/10.1088/1748-9326/7/1/015602, URL https://dx.doi.org/10.1088/1748-9326/7/1/015602.

Smith, D. M., and Coauthors, 2019: Robust skill of decadal climate predictions. *npj Climate and Atmospheric Science*, **2 (1)**, 1–10, https://doi.org/10.1038/s41612-019-0071-y, URL https://www.nature.com/articles/s41612-019-0071-y, number: 1 Publisher: Nature Publishing Group.

Smith, D. M., and Coauthors, 2020: North Atlantic climate far more predictable than models imply. *Nature*, **583 (7818)**, 796–800, https://doi.org/10.1038/s41586-020-2525-0, URL https://www.nature.com/articles/s41586-020-2525-0, number: 7818 Publisher: Nature Publishing Group.

Smith, D. M., and Coauthors, 2022: Robust but weak winter atmospheric circulation response to future Arctic sea ice loss. *Nature Communications*, **13 (1)**, 727, https://doi.org/10.1038/s41467-022-28283-y, URL https://www.nature.com/articles/s41467-022-28283-y, number: 1 Publisher: Nature Publishing Group.

Stringer, N., J. Knight, and H. Thornton, 2020: Improving Meteorological Seasonal Forecasts for Hydrological Modeling in European Winter. *Journal of Applied Meteorology and Climatology*, **59 (2)**, 317–332, https://doi.org/10.1175/JAMC-D-19-0094.1, URL https://journals.ametsoc.org/view/journals/apme/59/2/jamc-d-19-0094.1.xml, publisher: American Meteorological Society Section: Journal of Applied Meteorology and Climatology.

Strommen, K., 2020: Jet latitude regimes and the predictability of the North Atlantic Oscillation. *Quarterly Journal of the Royal Meteorological Society*, **146 (730)**, 2368–2391, https://doi.org/10.1002/qj.3796, URL https://onlinelibrary.wiley.com/doi/abs/10.1002/qj.3796, _eprint: https://onlinelibrary.wiley.com/doi/pdf/10.1002/qj.3796.

Strommen, K., and T. N. Palmer, 2019: Signal and noise in regime systems: A hypothesis on the predictability of the North Atlantic Oscillation. *Quarterly Journal of the Royal Meteorological Society*, **145 (718)**, 147–163, https://doi.org/10.1002/qj.3414, URL https://onlinelibrary.wiley.com/doi/abs/10.1002/qj.3414, _eprint: https://onlinelibrary.wiley.com/doi/pdf/10.1002/qj.3414.

Thornton, H. E., A. A. Scaife, B. J. Hoskins, D. J. Brayshaw, D. M. Smith, N. Dunstone, N. Stringer, and P. E. Bett, 2019: Skilful seasonal prediction of winter gas demand. *Environmental Research Letters*, **14 (2)**, 024 009, https://doi.org/10.1088/1748-9326/aaf338, URL https://dx.doi.org/10.1088/1748-9326/aaf338, publisher: IOP Publishing.

Thornton, H. E., D. M. Smith, A. A. Scaife, and N. J. Dunstone, 2023: Seasonal Predictability of the East Atlantic Pattern in Late Autumn and Early Winter. *Geophysical Research Letters*, **50 (1)**, e2022GL100 712, https://doi.org/10.1029/2022GL100712, URL https://onlinelibrary.wiley.com/doi/abs/10.1029/2022GL100712, _eprint: https://onlinelibrary.wiley.com/doi/pdf/10.1029/2022GL100712.

Woollings, T., A. Hannachi, and B. Hoskins, 2010: Variability of the North Atlantic eddy-driven jet stream. *Quarterly Journal of the Royal Meteorological Society*, **136 (649)**, 856–868, https://doi.org/10.1002/qj.625, URL https://onlinelibrary.wiley.com/doi/abs/10.1002/qj.625, _eprint: https://onlinelibrary.wiley.com/doi/pdf/10.1002/qj.625.

Woollings, T., B. Hoskins, M. Blackburn, and P. Berrisford, 2008: A New Rossby Wave–Breaking Interpretation of the North Atlantic Oscillation. *Journal of the Atmospheric Sciences*, **65 (2)**, 609–626, https://doi.org/10.1175/2007JAS2347.1, URL https://journals.ametsoc.org/view/journals/atsc/65/2/2007jas2347.1.xml, publisher: American Meteorological Society Section: Journal of the Atmospheric Sciences.

Zhang, W., B. Kirtman, L. Siqueira, A. Clement, and J. Xia, 2021: Understanding the signal-to-noise paradox in decadal climate predictability from CMIP5 and an eddying global coupled model. *Climate Dynamics*, **56 (9)**, 2895–2913, https://doi.org/10.1007/s00382-020-05621-8, URL https://doi.org/10.1007/s00382-020-05621-8.